Atomic Force Microscopy Study of Biaxially Oriented Polypropylene Films

H.-Y. Nie, M.J. Walzak, and N.S. McIntyre

Atomic force microscopy (AFM) uses a very sharp pointed mechanical probe to collect real-space morphological information of solid surfaces. AFM was used in this study to image the surface morphology of a biaxially oriented polypropylene film. The polymer film is characterized by a nanometer-scale, fiberlike network structure, which reflects the drawing process used during the fabrication of the film. AFM was used to study polymer-surface treatment to improve wettability by exposing the polymer to ozone with or without ultraviolet (UV) irradiation. Surface-morphology changes observed by AFM are the result of the surface oxidation induced by the treatment. Due to the topographic features of the polymer film, the fiberlike structure has been used to check the performance of the AFM tip. An AFM image is a mixture of the surface morphology and the shape of the AFM tip. Therefore, it is important to check the performance of a tip to ensure that the AFM image collected reflects the true surface features of the sample, rather than contamination on the AFM tip.

1. Introduction

Scanning-probe microscopy (SPM) is a relatively new family of microscopy techniques that can measure surface morphology. SPM originated from the scanning-tunneling microscopy (STM),[1,2] in which electrical current caused by the tunneling of electron through the tip and sample is used to maintain the distance between them. Because STM requires that the sample surface be conductive, atomic force microscopy (AFM)[3] was developed in 1986 to measure insulating surfaces. AFM has since developed very rapidly and has found various applications in many fields.

AFM provides a real-space, three-dimensional (3D) image of a surface through the detection of an interaction between a sharp mechanical tip and the surface features. Dependent on the operation mode of AFM, the interaction can be either a contact force, or an oscillation amplitude (which is then used as the feedback parameter to adjust the distance between the tip and the sample surface). The tip scans the sample surface, and the height information is obtained through the adjustment of the distance between them to keep the interaction constant. This technique requires almost no sample preparation and is able to obtain atomic spatial resolution.

Polypropylene (PP) is widely used in various areas, for example, from packaging to film capacitors. There have been reports of spherulitic structures on PP studied with scanning electron microscopy[4] and transmission electron microscopy.[5,6] AFM has been used to examine crystalline PP[6-8] and nanometer-scale fiber formation on shear-deformed isotactic[9] and hard elastic[10] PP surfaces. Recently, there have been studies on improving surface wettability on PP films using various surface modification techniques.[11,12]

The morphology of a biaxially oriented polypropylene (BOPP) film using AFM has been extensively studied.[13-19] The surface morphology of the BOPP film is characterized by a fiberlike network structure.[16] The nanometer-scale structure reflects the drawing process for fabricating the polymer film. AFM was also used to study changes in morphology and improvements in wettability caused[20-22] by exposing BOPP films to ozone with or without the presence of ultraviolet (UV) irradiation. Oxidation occurring on BOPP surfaces exposed to ozone alone is much slower than that introduced by the combination of ozone exposure and UV irradiation,[20,22] which provides an opportunity to monitor the difference in the speed of oxidation between a "normal" (i.e., untouched) BOPP surface and a scratched surface. The scratched surface has a higher[15] surface energy than the "normal" surface and indicates a preferential oxidation[17] on the scratched area. This paper shows that preferential oxidation is more clearly observed in the scratched area when exposed to ozone alone.

In the course of studying the BOPP film, the authors realized that its morphology could be used to check the integrity of the AFM tip.[18,19] An AFM image is, due to its imaging mechanism, a convolution of the tip geometry and the surface features. The sharper of either the AFM tip apex or the surface features acts as the effective probe. The *tip effect* is defined as a situation where the geometry of tip dominates the AFM image. It is thus necessary for one to check how accurately an AFM image reflects the surface features of the sample. Metal films and many other materials have been used to characterize AFM tips.[23] The advantage of using a polymer film instead of

H.-Y. Nie, M.J. Walzak, and **N.S. McIntyre,** Surface Science Western, Room G-1, Western Science Centre, The University of Western Ontario, London, Ontario N6A 5B7, Canada. Contact e-mail: hynie@ surf.ssw.uwo.ca.

those materials lies in the fact that the polymer surface is hydrophobic[24-26] and soft,[27] compared with silicon[28-30] AFM tips. These two properties are important for characterizing an AFM tip because they ensure that it is unlikely that the tip is contaminated or damaged in the verification process. The ability to collect AFM images in the same area on the BOPP film surface before and after a contaminated tip was cleaned allows[19] testing of the blind reconstruction[31-42] algorithm, by which tip geometry can be extracted solely from the image it collected.

2. Materials

Thermally extruded, biaxially oriented isotactic polypropylene film (3M Company, St. Paul, MN) was used in this study. The BOPP film (0.03 mm thick) was produced from a homopolymer resin (molecular weight $M_w = 1.9 \times 10^5$, polydispersity = 6.0). The base resin contains 500-1000 ppm each of an inorganic acid scavenger and a high-molecular-weight phenolic antioxidant. The polymer was produced on a tenter-frame film line and quenched at 45 °C prior to orientation. The film was formed with machine-draw (MD) and transverse-draw (TD) ratios of 5.2:1 and 9:1, respectively.

A sputtering system (Hummer VI, Technics EMS. Inc., Springfield, VA) was used to coat ~30 nm thick gold film on a BOPP film for the purpose of checking how a metal coating alters the morphology of the polymer surface.

To replicate "native" scratches seen on the BOPP film, local mechanical stresses (scratches) were created using a stylus-type surface profiler (P-10, Tencor, Santa Clara, CA), in which a diamond tip having a radius of ~2 μm was used to scan the film surface at a scan speed of 400 μm/s and a loading force of 0.4 mN. Variable forces of 0.1-0.5 mN were used to produce scratches with different widths.

BOPP films were treated by exposure to ozone flow (2 × 10^{17} molecule/cm^3), with and without the presence of UV irradiation, with primary lines at 184.9 and 253.7 nm. The flow rate of the ozone-containing air stream was 1000 sccm (standard cubic centimeters per minute) for UV/ozone treatment and 5000 (or 2000 as specified where applicable) sccm for the ozone-only treatment. Atomic oxygen formed from the photodecomposition of ozone in the presence of 253.7 nm UV irradiation is believed to be the main reactant resulting in oxidation and eventual scission of BOPP molecular chains.[20] Due to the lack of atomic oxygen in the ozone-only treatment, it has a much slower oxidation process, compared with the UV/ozone treatment.

3. Methods

A commercial AFM (Explorer, TopoMetrix, Santa Clara, CA) was used in this study. A sharp tip formed on the free end of a cantilever is used to probe the sample surface. The interaction between the tip and the surface is detected by measuring the deflection of the cantilever, using a laser diode to radiate the cantilever and a photodiode to detect the reflected laser beam. The quadrant photodiode is able to measure both the deflection and torsion of the cantilever. The principle of AFM is shown in Fig. 1.
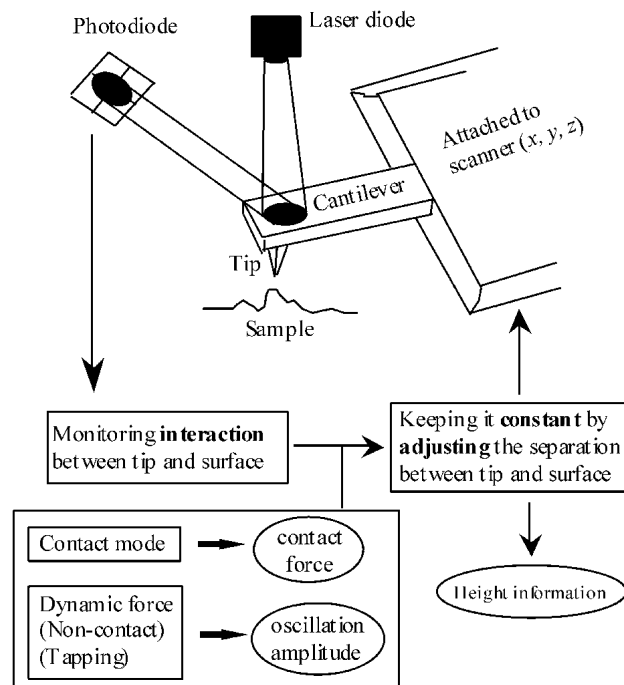

Fig. 1 Schematic illustration of AFM principle. While scanning the tip across the sample surface (x, y), the system adjusts the distance (z, which is thus the measure of the height of the sample surface features) between the tip and the sample surface to maintain a constant contact force (contact mode) or oscillation amplitude (dynamic-force mode). A 3D image is thus constructed by the lateral dimension that the tip scans and the height that the system measures.

Shown in Fig. 1 is a case where the tip scans the sample surface. The AFM operates by keeping constant the interaction between the tip and sample surface, using a feedback system that adjusts the distance between the tip and the sample surface. Depending on the interaction between the tip and sample surface, which is used as the feedback signal, there are two different imaging modes, described as follows.

3.1 Contact Mode

In the contact-mode AFM, the tip is in mechanical contact with the sample surface at a certain applied force. This applied force can be estimated from a force-distance curve, which is obtained by extending the tip to the surface to make contact between the tip and the surface, followed by retracting the tip from the surface. Shown in Fig. 2 is a force-distance curve obtained using a soft, silicon-nitride cantilever (spring constant: ~0.03 N/m). The cantilever was 0.6 μm thick, 18 μm wide, and 200 μm long, with an attached tip whose apex radius was nominally 20 nm.

The inserts shown in Fig. 2 depict the interaction between the tip and sample surface, which is detected by the deflection of the cantilever. There is no interaction between the tip and surface when the tip is far away from the surface [insert (a) in Fig. 2]. When the tip is brought close enough to the surface, there will be an attractive force between them. Usually, the gradient of the attractive force is much larger than the spring

constant of the cantilever, so that the tip is snapped to the surface to make a contact between the tip and surface (b). Extending the tip still further, a loading (repulsive) force acts on the surface (c). This repulsive force is usually used as the feedback parameter for the AFM system to obtain surface morphology. Forces of a couple of nN are used in contact-mode AFM. In the retracting cycle (d and e), due to the adhesion established after the contact between the tip and surface, the tip will not detach from the surface until the force used to pull the tip from the surface exceeds the adhesion force between them (f). This pull-off force can serve as a measure of the adhesion force between the tip and surface.[13,15,43-47]

When the tip scans the surface in contact-mode AFM, there is also a torsional movement of the cantilever that can be used to obtain further information on the interaction between the tip and surface. The measurement of this torsional movement may be referred to as lateral force imaging.[48] Lateral force imaging in AFM is usually used to image the distribution of different friction forces on a surface.[13,15,49-51] It has been shown that lateral force imaging can enhance topographic features,[14] which may be useful for surfaces where topographic images are difficult to obtain due to, for example, a large dynamic range for the height distribution of the sample surface. The arithmetical difference between the bidirectional lateral-force images results in a friction-force image, from which one is able to distinguish regions of higher hydrophilicity based on an increased interaction with the AFM tip. The direct output of the photodiode corresponding to the torsional movement of the cantilever (in units of nA) is the photo-induced current that was directly used to construct the lateral-force image.

3.2 Dynamic Force Mode

Dynamic-force (tapping or noncontact)-mode AFM, in which a cantilever oscillated around its resonant frequency is used to probe surface features, was developed initially to eliminate surface degradation encountered in contact-mode AFM, especially for soft materials.[52-55] For dynamic-force-mode AFM, silicon cantilevers with a spring constant of ~40 N/m were used. The cantilever was 125 μm long, 30 μm wide, and 3.7 μm thick. The tip apex radius was 10-20 nm. Because the variation of the oscillation amplitude is used in the feedback system (Fig. 3), the relative change of the oscillation amplitude of the cantilever (versus distance between the tip and sample surface) can be explained as follows.

Figure 3 shows that when the tip is far away from the sample surface [insert (a)], the oscillation amplitude of the cantilever is a constant, representing a "free-space" situation where there is no interaction between the tip and the surface. The amplitude decreases when the tip approaches close enough to the sample surface so that it "feels" attractive and/or repulsive forces (b). The cantilever stops oscillating when the tip is brought-in to mechanically contact the surface (c). Dynamic-force-mode AFM works by scanning the tip across the sample surface and adjusting the distance between the two through maintaining constant damped-oscillation amplitude of the cantilever, usually at 50% of the free-space oscillation.

All images were obtained in air with a typical relative humidity of about 50%. AFM images consisted of 500 lines with 500 points per line. Scan rates for smaller (up to 4 μm square)
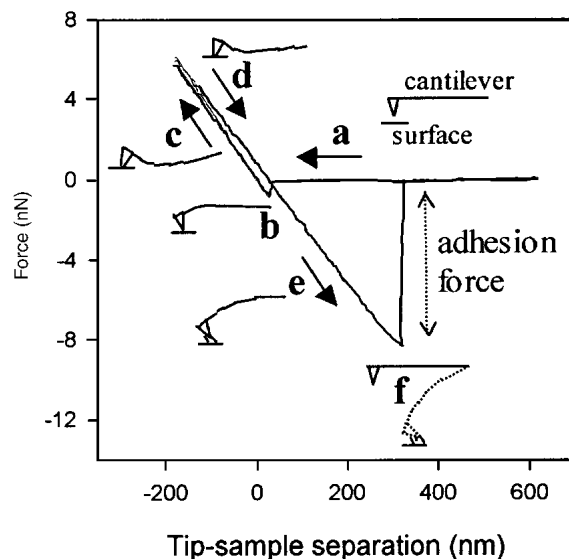
Fig. 2 A typical force-distance curve obtained on a BOPP film surface with a cantilever having a spring constant of 0.03 N/m. Interaction between the tip and the surface at different distance is indicated by **a-f**. Arrows guide the eye to the direction of the movement of the tip. Adhesion force between the tip and sample, due to their contact, can be measured as shown in the force-distance curve.
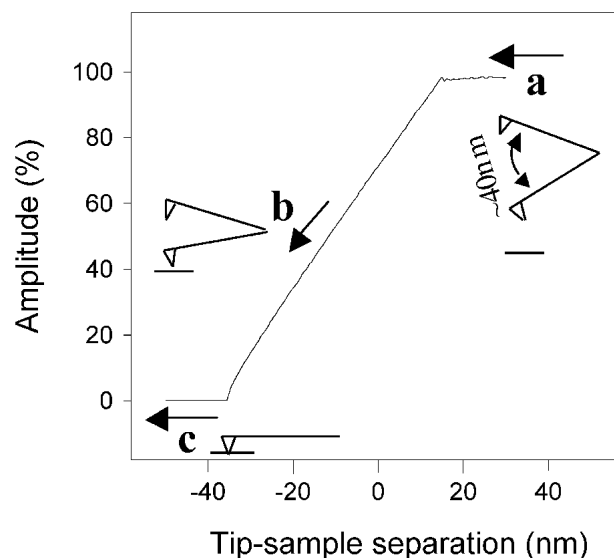
Fig. 3 An amplitude-distance curve obtained on a BOPP film surface. Interaction between the tip and the surface at different tip-sample distances is indicated by inserts **a-c**. Arrows indicate the direction of the tip approaching the sample surface.

and larger (over 5 μm square) areas were up to 10 and 50 μm/s, respectively. The images are in gray scale, where brighter areas represent higher areas.

3.3 Check Tip Performance

The BOPP film was used as a reference sample to check the performance of AFM tips. The simple criterion for judging a

tip is whether it can image the nanometer-scale fiberlike network structure.[18,19] When the tip is contaminated or damaged, the tip becomes larger than the BOPP fibers and the image will be dominated by tip effect.

Commercial software (SPIP, Metrology Image ApS, Denmark) can be used to estimate the geometry of the tip with its "tip characterization" module, in which the blind reconstruction algorithm[37,40] is implemented. The algorithm is based on the fact that surface features sharper than the tip actually act as a probe to image the AFM tip itself. The advantage of this method is that it uses solely a given image to deduce the tip geometry.

AFM images were obtained in the same area of the BOPP film using the same tip before and after it was contaminated. The difference in these images, thus, was solely induced by the contaminants on the tip apex. The shape of the contaminated tip was estimated from the image collected using the contaminated tip. This estimated tip geometry was in turn used to dilate the image collected by the clean tip; the outcome should resemble the image collected by the contaminated tip. This way, the performance of the software on estimating the tip shape from the image it collected can be tested.

4. Results and Discussion

4.1 Morphology of BOPP Film

AFM images obtained on BOPP films in an area of 20, 4, and 1 μm square are shown in Fig. 4(a)-(c). The image in Fig. 4(a) shows the overall morphology of the BOPP film. The MD direction is nominally the vertical direction of the image shown in this and all other images included in this article. Running in the MD direction, and approximately in the middle of the image, is a barely visible scratch 1-2 nm deep. Those scratches are strictly in the MD direction, and there is no end of a scratch ever observed through our extensive study on the morphology of the polymer film.[14,15]

Though not appearing in the particular area shown in Fig. 4(a), there are veins (larger fibers) running nominally in the MD direction for the particular BOPP film studied.[14,16] Figure 4(b) shows that the BOPP film surface is characterized by a fiberlike network structure. The nanometer-scale network structure is revealed very clearly in a close-up image of the polymer film (Fig. 4c). From the many AFM images collected on the BOPP film, the apparent size of the fibers ranges from 10-40 nm. As previously discussed, the network structure of the polymer fibers reflects the drawing process in which the BOPP film had been formed by stretching the original film. A different draw ratio results in a different morphology for the fiberlike network structure.[16]

Shown in Fig. 4(d) is the morphology of a sputter-coated gold film on a BOPP film. The morphology of the polymer surface has been altered significantly: the metal aggregates cover the surface, but leave cracks that most likely correspond to the ridges of the fibers. This result suggests that detailed surface structures of a polymer film can be easily altered if the polymer film is coated with a metal film. Although Fig. 4(d) shows a gold film of ~30 nm thick on a BOPP film, sputtering a gold film as thin as a couple of nm also altered the fine
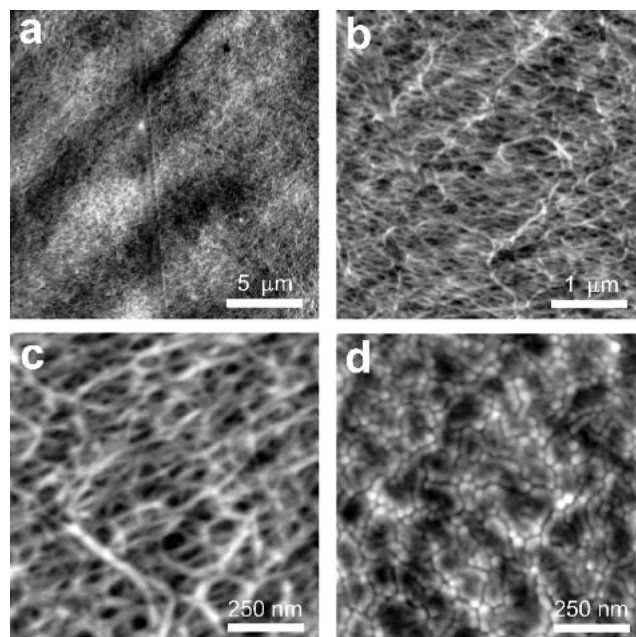

Fig. 4 Typical AFM images of BOPP films in a scan area of **(a)** 20 × 20 μm, **(b)** 4 × 4 μm, and **(c)** 1 × 1 μm. Shown in **(d)** is an AFM image (scan area, 1 × 1 μm) obtained after sputtering a gold film of 30 nm thick on the BOPP film. The gray scales are 49, 29, 12, and 16 nm for (a), (b), (c), and (d), respectively.

fiberlike network structure. It is thus clear that AFM is an excellent tool, capable of imaging the true surface morphology of the fine structure of polymer films.

The scratches found on the BOPP film are strictly in the MD direction and appear to arise from mechanical deformation in the rolling process, where the BOPP film had to go through many rollers. It is imaginable that if there were tiny protrusions on the rollers, their presence would result in mechanical deformation on the film surface when rolling the film through the rollers. Such localized forces produced the scratches observed.

To prove that these "native" scratches are indeed caused by such a mechanical deformation imposed by the protrusions on the rollers, experiments have been conducted reproducing the scratches on the BOPP film surface by scanning a diamond-tipped stylus across the polymer film.[15] Shown in Fig. 5(a) and (b) are a contact-mode AFM image and a friction-force image, respectively, simultaneously obtained on a BOPP film. The diamond tip had been used to produce an array of scratches by scanning the surface at an applied force of 0.4 mN and a speed of 400 μm/s. The five scratches clearly seen in the topographic image (Fig. 5a) are those produced by the stylus. Those scratches are approximately 10 nm deep and 1450 nm wide (as compared with the much shallower, 1-2 nm deep "native" scratches, which happen to be in the same area). The "native" scratches can barely be seen in the topographic image (Fig. 5a) due to their shallowness compared with the surface roughness. As clearly shown in the friction-force image (Fig. 5b), friction force measured on both the stylus-produced and "native" scratches are the same and larger than that on the "normal" areas. The adhesion force, which is a measure of surface energy of the sample surface,[15] measured on the
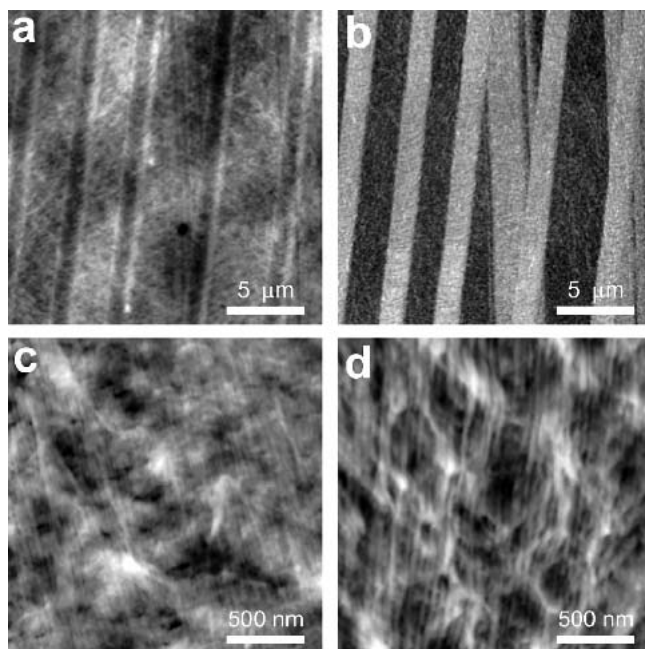
Fig. 5 (a) Topographic and (b) friction force images (scan area, 20 × 20 μm) for a BOPP film where native and stylus-induced scratches are seen. Shown in (c) and (d) are topographic images (scan area, 2 × 2 μm) for the native and stylus-produced scratches, respectively. The gray scales are 55, 19, and 15 nm for (a), (c), and (d), respectively. The gray scale for (b) is 5.38-7.85 nA, which is the (current) output of the photodiode for monitoring the friction force.

scratched area is also larger than that on the "normal" area. Increase in surface energy on the scratched area is proposed to be due to a buildup of extra free energy, which is transformed from part of the work done by the mechanical-scratching, in the form of increasing density and ordering of polymer molecular chains on the deformed surface.[15]

Shown in Fig. 5(c) and (d) are close-up images for a "native" and a stylus-produced scratch, respectively. It is clear that the polymer strands were reoriented to the scratching direction. By comparing AFM images for the scratches and the "normal" areas, the scratched areas show a much smaller corrugation height, indicating the scratched areas were also compressed. The contrast in the friction-force image suggests a higher surface energy for the scratched areas. The higher surface energy is believed to be due to the increased density and ordering of the polymer strands in the mechanically deformed areas.[15]

Shown in Fig. 6 are apparent widths of the scratches created using different applied forces. At larger applied forces, there were pileups at the edges of the scratch, apparently a result of the accumulation of the polymer material introduced in the course of the scratching. The widths presented in Fig. 6 for the scratches created at larger applied forces were estimated by including the pileups. This estimation method was used for showing the overall size of the scratches and may result in an overestimate for the actual contact area between the tip and the polymer film. The scratch created on the polymer film is likely the result of a combination of elastic and plastic deformations.[56]

As shown in Fig. 5(a) and (b), the stylus-produced scratches have the same width because the conditions to make them are
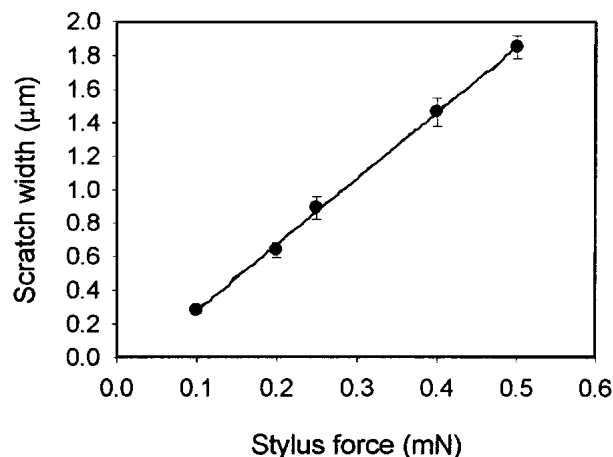

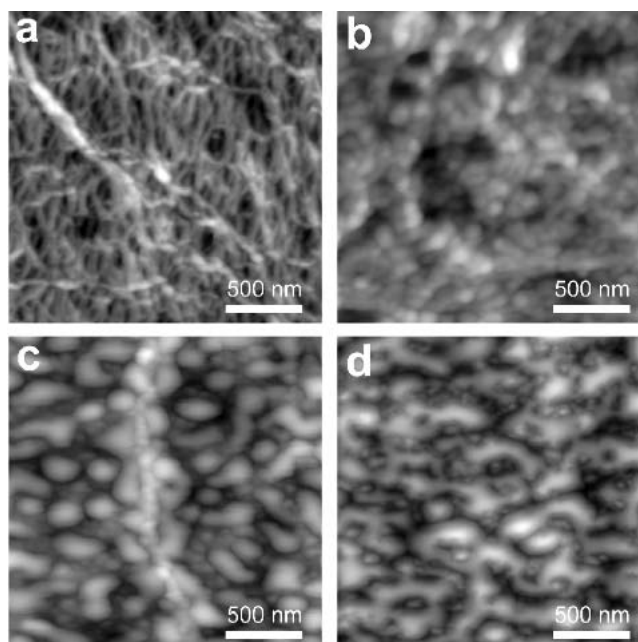Fig. 6 Width of scratches produced by a diamond-tipped stylus as a function of the applied force

Fig. 7 Topographic images (scan area, 2 × 2 μm) for BOPP films subjected to UV/ozone treatment for (a) 1 min, (b) 4 min, (c) 15 min, and (d) 45 min. The gray scales are 33, 31, 32, and 39 nm for (a), (b), (c), and (d), respectively.

identical. In contrast, the "native" scratches observed in this area and other areas (not shown) have various widths, suggesting that the length and/or the size of the protrusions on the rollers are diverse. One can expect that the "native" scratches, such as those observed for the BOPP film, will probably disappear with the removal of such protrusions from the rollers.

4.2 UV/Ozone and Ozone-Only Treatments

Shown in Fig. 7(a) is an AFM image obtained on a 1 min UV/ozone-treated BOPP film. Adhesion force measurement

showed a clear increase in surface energy on this treated surface,[15] indicating that the chemistry of the surface was modified by the treatment. This adhesion-force measurement using AFM[15] is consistent with previous measurements using x-ray photoelectron spectroscopy (XPS) and contact-angle method, in which an uptake of oxygen and a decrease in contact angle was observed, respectively, for 1 min UV/ozone-treated BOPP samples.[20]

However, the fiberlike feature remains after this 1 min UV/ozone treatment. It is believed that there are oxygen-containing functional groups formed on the surface, which accounts for the observed chemistry change on the surface. The oxidation is thus insufficient for breaking the polymer chains to form low molecular weight oxidized material (LMWOM).

After an UV/ozone treatment for 4 min (Fig. 7b), the surface morphology changed completely: nodulelike features emerged. This morphology change is the result of oxidation of the polymer surface, resulting in the formation of LMWOM (including carbonyls, carboxylic acids, hydroxyl-group, and many other oxygen-related groups).[20] Increasing the treatment time resulted in the formation of larger mounds on the surface. Shown in Fig. 7(c) is an AFM image for a 15 min UV/ozone-treated BOPP film surface. Compared with the nodulelike features seen on the 4 min treated sample, the 15 min treated sample shows elongated droplets. It is reasonable to assume that as the treatment time is increased, more LMWOM is produced. The greater volume of LMWOM allows it to accumulate to form larger droplets.[17]

Morphology changes and the formation of LMWOM have been clearly shown by AFM. Another aspect of the formation of LMWOM is the increase in water wettability, as previously determined from contact-angle measurements.[20] An additional advantage in using AFM to investigate modified polymer surfaces is that AFM also provides information on changes in the adhesion force at the surface. The adhesion force was found to increase with increasing treatment time.[13,17] The increase in adhesion force indicates an increase in surface energy. The surface energy increase for the UV/ozone-treated BOPP film is a direct result of the oxidation of the polymer surface, resulting in polar oxidized materials.[20]

An extended UV/ozone treatment for 45 min resulted in yet another change in morphology. As shown in Fig. 7(d), the surface morphology is now characterized by connected droplets. This finding suggests that, as more LMWOM is produced, the resultant droplets contact and coalesce. The morphology shown in Fig. 7(d) indicates a relatively small difference of surface energy between the underlying surface and the droplets, because the droplets have spread out on the underlying surface.

The oxidized material (LMWOM) forming the droplets is found to be water washable, suggesting that they are soluble in water. However, washing does not restore the fiberlike structure of the pristine BOPP film, indicating that the underlying surface is covered by moderately oxidized materials that are insoluble in water.[17] Because this underlying surface still displays higher surface energy, the improvement of wettability is preserved even after washing the UV/ozone-treated surface.

It has been established that UV/ozone treatment modifies the polymer surface quickly. UV irradiation is believed to provide reactive atomic oxygen through photo-decomposition of

ozone.[20] XPS has been used to measure the uptake of oxygen on the ozone and UV/ozone-treated BOPP film samples. O/C ratios calculated from the XPS measurement show that the oxygen uptake is much lower and slower for the ozone treatment than for the UV/ozone treatment.[20] The preferential oxidation in the scratched area for UV/ozone treatment has been previously reported, as judged from the difference in the size of the mounds between the scratched and "normal" areas.[17] To see how different the oxidation would be if no such reactive atomic oxygen were generated, experiments were conducted using ozone without the presence of the UV irradiation to treat the polymer film. Shown in Fig. 8 are AFM images for BOPP films subjected to ozone exposure (the ozone flow rate was 5000 sccm), without UV irradiation for different periods of time.

Figure 8(a) is a reference image of a BOPP film without the treatment. As shown in Fig. 8(b), BOPP films subjected to 10 min ozone treatment show no significant change in morphology. Even after an ozone treatment for 30 min, the fiberlike network structure is still visible (Fig. 8c). After exposing a BOPP film to ozone for 45 min, the surface morphology of the
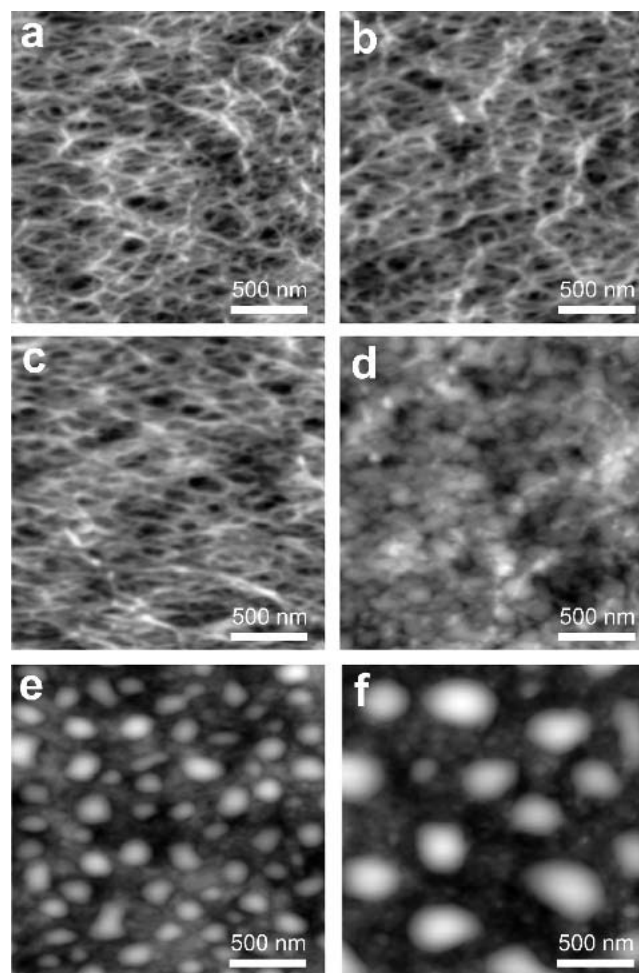

Fig. 8 Topographic images (scan area, 2×2 μm) for BOPP films subjected to ozone-only treatment for **(a)** 0 min, **(b)** 10 min, **(c)** 30 min, **(d)** 45 min, **(e)** 60 min, and **(f)** 120 min. The gray scales are 25, 26, 18, 21, 25, and 43 nm for (a), (b), (c), (d), (e), and (f), respectively.
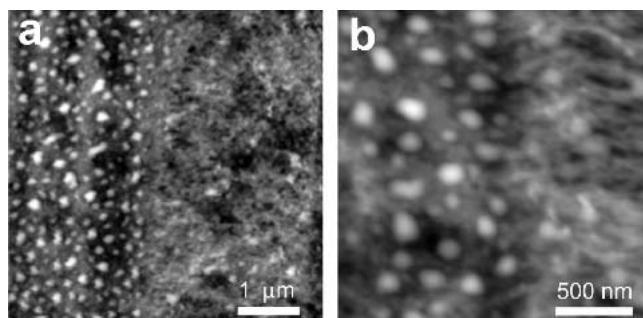
Fig. 9 Topographic images for ozone-only treated BOPP film in an area of **(a)** 5 × 5 µm and **(b)** 2 × 2 µm, showing preferential oxidation in scratched area. The gray scales are 36 and 20 nm for (a) and (b), respectively.
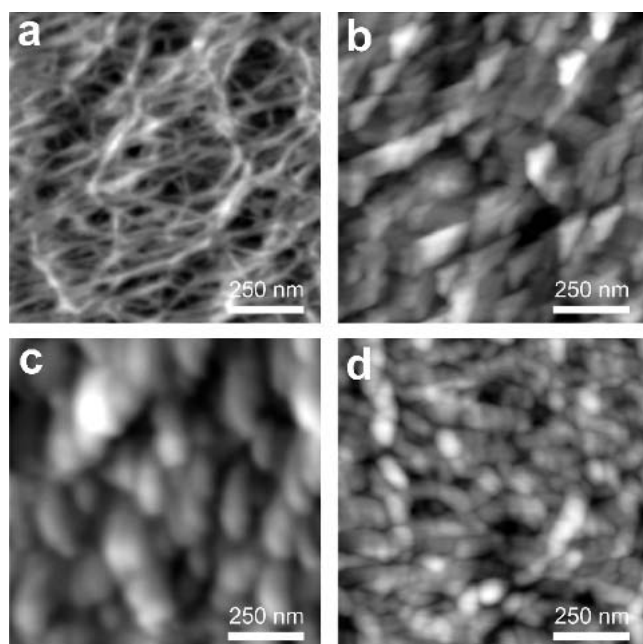

Fig. 10 Topographic images (scan area, 1 × 1 µm) for BOPP films obtained by **(a)** a clean tip, **(b)** a damaged tip, **(c)** another damaged tip, and **(d)** a contaminated tip. The gray scales are 19 nm for all images.

polymer film starts showing the formation of nodules (Fig. 8d). Compared with UV/ozone treatment, the ozone-only treatment is much slower in modifying the morphology of the polymer surface. Therefore, UV irradiation plays an important role in the oxidation of the polymer surface for the UV/ozone treatment. As investigated from other techniques, atomic oxygen generated through a photo-decomposition process induced by UV irradiation is the key for quickly modifying the polymer surface.[20]

When the ozone treatment time was increased to 60 min, well-separated droplets emerged on the polymer surface (Fig. 8e). Compare Fig. 7(c) and 8(e); the size of the droplets for the 15 min UV/ozone treated and 60 min ozone-treated surface is similar. However, the ozone-treated surface shows round and well-separated droplets, in contrast to the elongated and more closely packed droplets on the UV/ozone-treated surface. Fig-

ure 8(f) is an AFM image for the morphology of a BOPP film treated by ozone for 120 min, showing the formation of large droplets that are separated from each other. It appears that the droplets induced by ozone treatment grow with increasing treatment time but remain separated. This result is in contrast to those observed for UV/ozone treated samples, as shown in Fig. 7(d). The difference in morphology suggests that the oxidized materials from the two different treatments may be different.

Shown in Fig. 9 are two AFM images for the ozone-only treatment of BOPP films (the ozone flow rate was 2000 sccm), displaying preferential oxidation in the scratched area as evidenced by the formation of droplets in the scratched area, but not in the "normal" area. The scratched area is at the left-hand side of the image shown in Fig. 9(a). Differences in the oxidation in the scratched and "normal" areas are clearly depicted in the image. Figure 9(b) shows a close-up image for the scratched area at the left-hand side and the "normal" area at the right-hand side, respectively. It was confirmed that the mounds produced by ozone-only treatment are removed by water washing, similar to those produced by UV/ozone treatment.

AFM measurements show that the change in the surface structures is accompanied by a change in surface energy.[15] Increase in surface energy caused by the mechanical deformation may have an implication for understanding the surface modifications of polymer. Figure 9 shows preferential oxidation in the scratched area. This result is attributed to the fact that the scratched area has a higher initial surface energy, making it more amenable to oxidation.

4.3 Check Tip Performance Using the BOPP Film

Shown in Fig. 10(a) is an AFM image obtained on a BOPP film using a clean tip, reflecting the true morphology characterized by the fiberlike network structure. When damaged or contaminated AFM tips were used, the fiberlike features are no longer seen in the AFM images (Fig. 10b-d). The three images are obviously dominated by three different tip shapes. AFM images in Fig. 10 strongly suggest that the BOPP film can be used as a reference sample to check the performance of an AFM tip. The criterion is simple and straightforward: if the fiberlike features are revealed by an AFM tip, then the tip quality is sufficient to collect "true" images.[18,19] An AFM tip can be easily contaminated or damaged depending on the chemical and mechanical properties of the sample surface it scans.[57] It is therefore desirable to adopt a simple qualifying method, such as the one using BOPP film, to check the performance of AFM tips.

To prove that BOPP film is indeed useful for checking AFM tip performance, images from the same area were obtained using the same tip when it was clean, after it had been contaminated, and then after it was cleaned again. That way, any change in the AFM images obtained would be solely due to the contamination on the tip apex. Two tips were contaminated by scanning two specially prepared samples.[19] Shown in Fig. 11 are two sets of AFM images for two different contaminated tips. The first set of AFM images shown in Fig. 11(a), (c), and (e) were obtained on the same area using a tip when it was clean, contaminated, and recleaned, respectively. The tip used for Fig. 11(c) was contaminated by scanning a sample surface that was UV/ozone-treated, followed by water washing.[18,19] It is clear
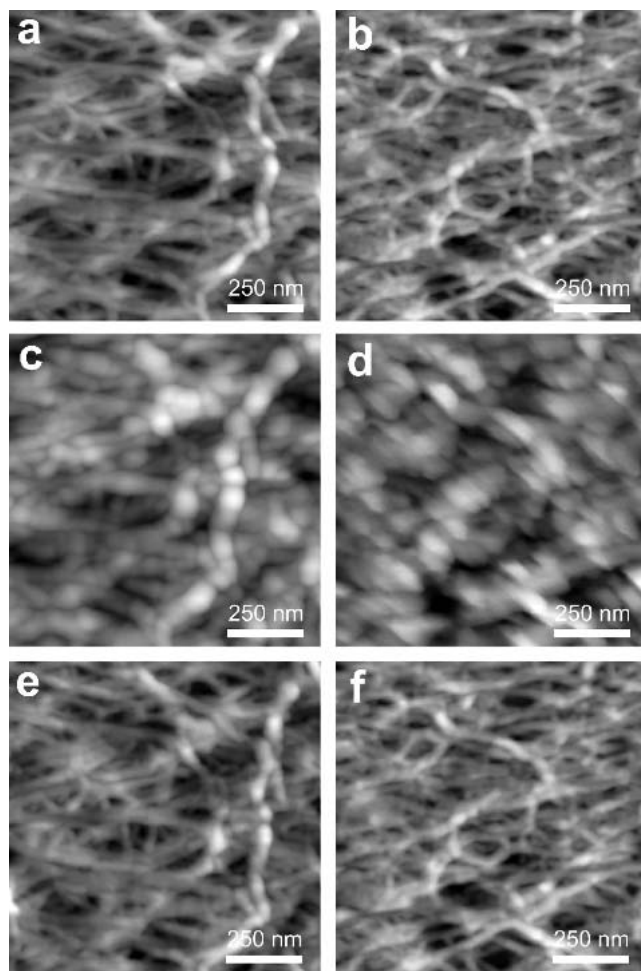
Fig. 11 Topographic images (scan area, 1 × 1 μm) obtained on the same BOPP area when the same AFM tip was **(a)** clean, **(c)** contaminated, and **(e)** cleaned. Another example using a differently contaminated tip is shown in **(b), (d)**, and **(f)**. The gray scales are 31, 24, 29, 15, 29, and 24 nm for (a), (b), (c), (d), (e), and (f), respectively.

Fig. 12 **(a)** and **(b)** are geometry of the contaminated tips estimated from the images of Fig. 11(c) and (d), respectively. The lateral dimensions for (a) and (b) are 168 × 168 nm; the gray scales are 24 and 14 nm for (a) and (b), respectively. **(c)** and **(d)** are dilated images (scan area, 1 × 1 μm) from Fig. 11(a) and (b) using the tip shown in (a) and (b), respectively.

that the image collected by the contaminated tip is dominated by tip effect (Fig. 11c).

The contaminated tip was cleaned by pushing it into the polymer film, and its cleanliness is evidenced in AFM image shown in Fig. 11(e). An amplitude-distance curve, such as the one shown in Fig. 3, is used to control how deeply the tip is pushed into the polymer surface. The depth can be controlled by counting from the distance where the cantilever stopped oscillating. In the course of pushing the tip into the polymer film, the behavior of the contaminant may be reflected in the amplitude-distance curve as it is being removed from the tip apex.[18]

Shown in Fig. 11(b), (d), and (f) are AFM images using another contaminated tip on another BOPP film sample, when the tip was clean, contaminated, and cleaned, respectively. By comparing Fig. 11(c) and (d), it is clear that this tip was contaminated differently from the one described previously. In fact, this tip was contaminated by being scanned on an organic acid[58] coated Si substrate.[19] Once again, the use of the BOPP film to check the AFM tip performance and to clean the contaminated tip was successful.
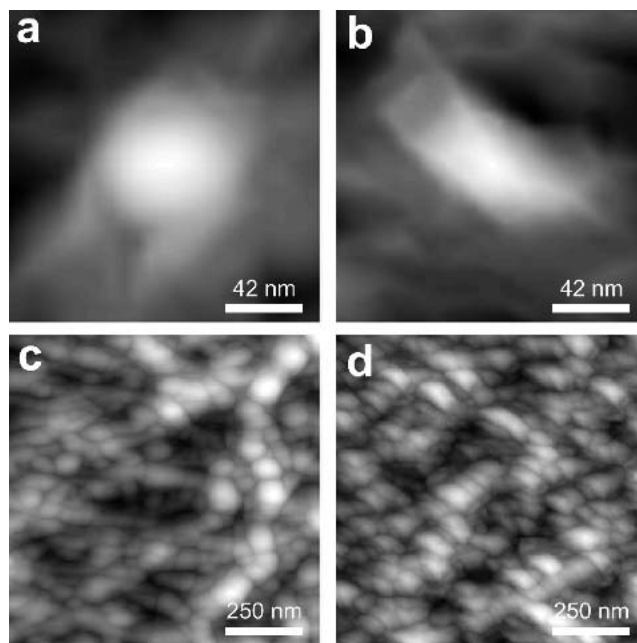
For contaminated tips used to collect AFM images in Fig. 11, pushing them into the polymer film cleaned them. If a tip was damaged, pushing the tip into the polymer would not result in a better tip. If uncertain about whether a tip is contaminated or damaged, UV/ozone treatment of the tip for half an hour usually answers the question; most organic contamination would be removed by the UV/ozone treatment. Based on this procedure, tips corresponding to images shown in Fig. 10(b) and (c) were damaged, and the one corresponding to Fig. 10(d) was contaminated.

The ability to image the same area of the BOPP film before and after the same tip was contaminated was used to test commercial software in which the algorithm of blind reconstruction for extracting the tip shape was implemented. The difference in such AFM images is solely due to the tip contamination. The contaminated tip can be estimated from the image it collected. Shown in Fig. 12(a) and (b) are topographic images for the geometry of the tip estimated from Fig. 11(c) and (d), respectively. According to the tip shape estimated from the image in Fig. 11(c), the upper bond of the contaminant on the tip is basically round and has a radius of ~80 nm, compared to the nominal radius of 10-20 nm for a clean tip.

Figure 12(b) shows a differently shaped contaminant estimated from Fig. 11(d). This contaminant is elongated 90 nm across the elongated direction. The apparent height for the contaminant shown in Fig. 12(a) and (b) is 20 and 14 nm, respectively. This apparent height is most likely underestimated for the contaminant, because the limited height of the surface features of the BOPP film only images the top of the tip apex. The flat outlying areas in Fig. 12(a) and (b) are artifacts reflecting this limitation.

The blind-reconstruction algorithm extracts the AFM tip shape solely from the AFM image collected by the tip. Dilation is a mathematical operation that convolutes the tip effect to an existing image, which simulates the AFM imaging mechanism. A simple way to test blind reconstruction was derived, based on dilation of a tip geometry into an image and the ability to image the same area of the BOPP film surface using the same tip before and after it was contaminated. This method uses comparison of the AFM image collected using the contaminated tip (Fig. 11c or d) and the dilated image (Fig. 12c or d), from the image collected using the clean tip (Fig. 11a or b). If the estimation of the contaminated-tip geometry is reasonable, then one expects to be able to use the estimated tip geometry to dilate the image collected, using the clean tip to obtain an image resembling one collected using the contaminated tip. Shown in Fig. 12(c) and (d) are dilated images from Fig. 11(a) and (b) using the estimated contaminated-tip geometry shown in Fig. 12(a) and (b), respectively. It is clear that the dilated images resemble the images collected using the contaminated tips. Therefore, the blind construction algorithm successfully extracts the geometry of the contaminated tip.

5. Conclusions

Nanometer-scale morphology of a BOPP film and its surface modification by UV/ozone and ozone-only treatments were investigated using AFM. Surface modification by UV/ozone treatment was found to be much faster than that by ozone-only treatment, consistent with the oxygen-uptake measurements by XPS. Investigations on scratches produced by force-controlled diamond tip (using a stylus profiler) showed that the native scratches on the polymer film are due to mechanical deformation occurring in the rolling process (in which protrusions on rollers are most likely the source for such mechanical forces). Preferential oxidation was observed on scratched areas, indicating that the scratched areas have a higher surface energy and hence are more amenable to surface modification by ozone or UV/ozone treatment.

The nanometer-scale fiberlike network structure of the BOPP film surface was useful in checking AFM tip performance. This utility is because the size of the fibers is close to the apex radius of clean tips, but smaller than a contaminated tip. The ability to collect images of the same areas using the same tip (when it was clean and contaminated) provided a simple way to test the blind-reconstruction algorithm, which allows one to extract tip geometry solely from the image it collected.

References

1. G. Binnig, H. Rohrer, Ch. Gerber, and E. Weibel: "Tunneling Through a Controllable Vacuum Gap," *Appl. Phys. Lett.,* 1982, *40,* pp. 178-80.
2. G. Binnig, H. Rohrer, Ch. Gerber, and E. Weibel: "Surface Studies by Scanning Tunneling Microscopy," *Phys. Rev. Lett.,* 1982, *49,* pp. 57-61.
3. G. Binnig, C.F. Quate, and Ch. Gerber: "Atomic Force Microscope," *Phys. Rev. Lett.,* 1986, *56,* pp. 930-33.
4. M. Aboulfaraj, B. Ulrich, A. Dahoun, and C. G'Sell: "Spherulitic Morphology of Isotactic Polypropylene Investigated by Scanning Electron-Microscopy," *Polymer,* 1993, *34,* pp. 4817-25.
5. R.A. Campbell, P.J. Phillips, and J.S. Lin: "The Gamma-Phase of High-Molecular-Weight Polypropylene; 1. Morphological Aspects," *Polymer,* 1993, *34,* pp. 4809-16.
6. W. Stocker, M. Schumacher, S. Graff, J. Lang, J.C. Wittmann, A.J. Lovinger, and B. Lotz: "Direct Observation of Right and Left Helical Hands of Syndiotactic Polypropylene by Atomic-Force Microscopy," *Macromolecules,* 1994, *27,* pp. 6948-55.
7. D. Snetivy and G.J. Vancso: "Atomic-Force Microscopy of Polymer Crystals; 7. Chain Packing, Disorder and Imaging of Methyl-Groups in Oriented Isotactic Polypropylene," *Polymer,* 1994, *35,* pp. 461-67.
8. V.V. Tsukruk and D.H. Reneker: "Surface-Morphology of Syndiotactic Polypropylene Single-Crystals Observed by Atomic-Force Microscopy," *Macromolecules,* 1995, *28,* pp. 1370-76.
9. G. Castelein, G. Coulon, and C. G'Sell: "Polymers Under Mechanical Stress: Deformation of the Nanostructure of Isotactic Polypropylene Revealed by Scanning Force Microscopy," *Polym. Eng. Sci.,* 1997, *37,* pp. 1694-701.
10. S. Hild, W. Gutmannsbauer, R. Luthi, J. Fuhrmann, and H.-J. Gruntherodt: "A Nanoscopic View of Structure and Deformation of Hard Elastic Polypropylene With Scanning Force Microscopy," *J. Polym. Sci.: Polym. Phys.,* 1996, *34,* pp. 1953-59.
11. R.M. Overney, R. Luthi, H. Haefke, J. Frommer, E. Meyer, H.-J. Gruntherodt, S. Hild, and J. Fuhrmann: "An Atomic Force Microscopy Study of Corona-Treated Polypropylene Films," *Appl. Surf. Sci.,* 1993, *64,* pp. 197-203.
12. M. Strobel, V. Jones, C.S. Lyons, M. Ulsh, M.J. Kushner, R. Dorai, and M.C. Branch: "A Comparison of Corona-Treated and Flame-Treated Polypropylene Films," *Plasmas Polym.,* 2003, *8,* pp. 61-95.
13. H.-Y. Nie, M.J. Walzak, B. Berno, and N.S. McIntyre: "Atomic Force Microscopy Study of Polypropylene Surfaces Treated by UV and Ozone: Modification of Morphology and Adhesion Force," *Appl. Surf. Sci.,* 1999, *144-145,* pp. 627-32.
14. H.-Y. Nie, M.J. Walzak, N.S. McIntyre, and A.M. EL-Sherik: "Applications of Lateral Force Imaging to Enhance Topographic Features of Polypropylene Film and Photo-cured Polymers," *Appl. Surf. Sci.,* 1999, *144-145,* pp. 633-37.
15. H.-Y. Nie, M.J. Walzak, B. Berno, and N.S. McIntyre: "Microscopic Stripe Formation and Adhesion Force Increase Introduced by Local Shear-Stress Deformation of Polypropylene Film," *Langmuir,* 1999, *15,* pp. 6484-89.
16. H.-Y. Nie, M.J. Walzak, and N.S. McIntyre: "Draw-Ratio-Dependent Morphology of Biaxially-Oriented Polypropylene Films as Determined by Atomic Force Microscopy," *Polymer,* 2000, *41,* pp. 2213-18.
17. H.-Y. Nie, M.J. Walzak, and N.S. McIntyre: "Atomic Force Microscopy Study of UV/ozone Treated Polypropylene Films," *Polymer Surface Modification: Relevance to Adhesion,* Vol. 2, K.L. Mittal, ed., VSP, Utrecht, The Netherlands, 2000, pp. 377-92.
18. H.-Y. Nie and N.S. McIntyre: "A Simple and Effective Method of Evaluating Atomic Force Microscopy Tip Performance," *Langmuir,* 2001, *17,* pp. 432-36.
19. H.-Y. Nie, M.J. Walzak and N.S. McIntyre: "Use of Biaxially-Oriented Polypropylene Film for Evaluating and Cleaning Contaminated Atomic Force Microscopy Probe Tips: An Application to Blind Tip Reconstruction," *Rev. Sci. Instrum.,* 2002, *73,* pp. 3831-36.
20. M.J. Walzak, S. Flynn, R. Foerch, J.M. Hill, E. Karbashewski, A. Lin, and M. Strobel: "UV and Ozone Treatment of Polypropylene and Poly(ethylene-terephthalate)," *J. Adhesion Sci. Technol.,* 1995, *9,* pp. 1229-48.
21. J.M. Hill, E. Karbashewski, A. Lin, M. Strobel, and M.J. Walzak: "Effects of Aging and Washing on UV and Ozone-Treated Poly(ethylene terephthalate) and Polypropylene," *J. Adhesion Sci. Technol.,* 1995, *9,* pp. 1575-91.
22. M. Strobel, M.J. Walzak, J.M. Hill, A. Lin, E. Karbashewski, and C.S. Lyons: "A Comparison of Gas-Phase Methods of Modifying Polymer Surfaces," *J. Adhesion Sci. Technol.,* 1995, *9,* pp. 365-83.
23. D. Vick, M.J. Brett and K. Westra: "Porous Thin Films for the Characterization of Atomic Force Microscope Tip Morphology," *Thin Solid Films,* 2002, *408,* pp. 79-86, and references therein.
24. C.J. van Oss, M.K. Chaudhury, and R.J. Good: "The Mechanism of Phase-separation of Polymers in Organic Media—Apolar and Polar Systems," *Sep. Sci. Technol.,* 1989, *24,* pp. 15-30.
25. S. Wu: *Polymer Interface and Adhesion,* Marcel Dekker, New York, 1982, Chapter 5.

26. H. Schonhorn and L.H. Sharpe: "Surface Tension of Molten Polypropylene," *J. Polym. Sci. Part B: Polym. Lett.,* 1965, *3,* pp. 235-37.
27. W. Brostow, J. Kubat, and M.M. Kubat: "Mechanical Properties," *Physical Properties of Polymers Handbook,* J.E. Mark, ed., American Institute of Physics, New York, 1996, pp. 313-34.
28. L.M. Zhang, D. Uttamchandani, and B. Culshaw: "Measurement of the Mechanical-Properties of Silicon Microresonators," *Sensors and Actuators A,* 1991, *29,* pp. 79-84.
29. K.E. Petersen: "Silicon as a Mechanical Material," *Proceedings of the IEEE,* 1982, *70,* pp. 420-57.
30. J.J. Wortman and R.A. Evans: "Young's Modulus, Shear Modulus, and Poisson's Ratio in Silicon and Germanium," *J. App. Phys.,* 1965, *36,* pp. 153-56.
31. P. Markiewicz and M.C. Goh: "Atomic-Force Microscopy Probe Tip Visualization and Improvement of Images Using a Simple Deconvolution Procedure," *Langmuir,* 1994, *10,* pp. 5-7.
32. J. Vesenka, R. Miller, and E. Henderson: "Three-Dimensional Probe Reconstruction for Atomic Force Microscopy," *Rev. Sci. Instrum.,* 1994, *65,* pp. 2249-51.
33. J.S. Villarrubia: "Morphological Estimation of Tip Geometry for Scanned Probe Microscopy," *Surf. Sci.,* 1994, *321,* pp. 287-300.
34. P. Markiewicz and M.C. Goh: "Atomic-Force Microscope Tip Deconvolution Using Calibration Arrays," *Rev. Sci. Instrum.,* 1995, *66,* pp. 3186-90.
35. P. Markiewicz and M.C. Goh: "Simulation of Atomic-Force Microscope Tip-Sample Sample-Tip Reconstruction," *J. Vac. Sci. & Technol. B,* 1995, *13,* pp. 1115-18.
36. S. Dongmo, M. Troyon, P. Vautrot, E. Delain, and N. Bonnet: "Blind Restoration Method of Scanning Tunneling and Atomic Force Microscopy Images," *J. Vac. Sci. & Technol. B,* 1996, *14,* pp. 1552-56.
37. P.M. Williams, K.M. Shakesheff, M.C. Davies, D.E. Jackson, C.J. Roberts, and S.J.B. Tendler: "Blind Reconstruction of Scanning Probe Image Data," *J. Vac. Sci. & Technol. B,* 1996, *14,* pp. 1557-62.
38. J. Vesenka, T. Marsh, R. Miller, and E. Henderson: "Atomic Force Microscopy Reconstruction of G-Wire DNA," *J. Vac. Sci. & Technol. B,* 1996, *14,* pp. 1413-17.
39. M.F. Tabet and F.K. Urban: "Deconvolution of Tip Affected Atomic Force Microscope Images and Comparison to Rutherford Backscattering," *J. Vac. Sci. & Technol. B,* 1997, *15,* pp. 800-04.
40. J.S. Villarrubia: "Algorithms for Scanned Probe Microscope Image Simulation, Surface Reconstruction, and Tip Estimation," *J. Res. Natl. Inst. Stan.,* 1997, *102,* pp. 425-54.
41. L.S. Dongmo, J.S. Villarrubia, S.N. Jones, T.B. Renegar, M. Postek, and J.F. Song: "Experimental Test of Blind Tip Reconstruction for Scanning Probe Microscopy," *Ultramicroscopy,* 2000, *85,* pp. 141-53.
42. A. Todd and S.J. Eppell: "A Method to Improve the Quantitative Analysis of SFM Images at the Nanoscale," *Surf. Sci.,* 2001, *491,* pp. 473-83.
43. H.A. Mizes, L.-G. Loh, R.J. Miller, S.K. Ahuja, and E.F. Grabowski: "Submicron Probe of Polymer Adhesion With Atomic Force Microscopy—Dependence on Topography and Material Inhomogeneities," *Appl. Phys. Lett.,* 1991, *59,* pp. 2901-03.
44. M. Radmacher, M. Fritz, J.P. Cleveland, D.A. Walters, and P.K. Hansma: "Imaging Adhesion Forces and Elasticity of Lysozyme Adsorbed on Mica With the Atomic-Force Microscope," *Langmuir,* 1994, *10,* pp. 3809-14.
45. G. Toikka, R.A. Hayes, and J. Ralston: "Adhesion of Iron Oxide to Silica Studied by Atomic Force Microscopy," *J. Colloid Interface Sci.,* 1996, *180,* pp. 329-38.
46. E.W. van der Vegte and G. Hadziioannou: "Scanning Force Microscopy with Chemical Specificity: An Extensive Study of Chemically Specific Tip-Surface Interactions and the Chemical Imaging of Surface Functional Groups," *Langmuir,* 1997, *13,* pp. 4357-68.
47. K. Feldman, T. Tervoort, P. Smith, and N.D. Spencer: "Toward a Force Spectroscopy of Polymer Surfaces," *Langmuir,* 1998, *14,* pp. 372-28.
48. G. Meyer and N. Amer.: "Simultaneous Measurement of Lateral and Normal Forces With an Optical-Beam-Deflection Atomic Force Microscope," *Appl. Phys. Lett.,* 1990, *57,* pp. 2089-91.
49. R.M. Overney, E. Meyer, J. Frommer, D. Brodbeck, R. Luthi, L. Howald, H.-J. Guntherodt, M. Fujihira, H. Takano, and Y. Goto: "Friction Measurements on Phase-Separated Thin-Films With a Modified Atomic Force Microscope," *Nature,* 1992, *58,* pp. 133-35.
50. Y.F. Dufrene, W.R. Barger. J.-B.D. Green, and G.U. Lee: "Nanometer-Scale Surface Properties of Mixed Phospholipid Monolayers and Bilayers," *Langmuir,* 1997, *13,* pp. 4779-84.
51. M. Motomatsu, H.-Y. Nie, W. Mizutani, and H. Tokumoto: "Local Properties of Phase-Separated Polymer Surfaces by Force Microscopy," *Jpn. J. Appl. Phys.,* 1994, *33,* pp. 3775-78.
52. Q. Zhong, D. Inniss, K. Kjoller, and V.B. Elings: "Fractured Polymer Silica Fiber Surface Studied by Tapping Mode Atomic-Force Microscopy," *Surf. Sci.,* 1993, *290,* pp. L688-92.
53. J.P. Spatz, S. Sheiko, M. Moller, R.G. Winkler, P. Reineker, and P. Marti: "Forces Affecting the Substrate in Resonant Tapping Force Microscopy," *Nanotechnology,* 1995, *6,* pp. 40-44.
54. J. Tamayo and R. Garcia: "Deformation, Contact Time, and Phase Contrast in Tapping Mode Scanning Force Microscopy," *Langmuir,* 1996, *12,* pp. 4430-35.
55. N.A. Burnham, O.P. Behrend, F. Oulevey, G. Gremaud, P.-J. Gallo, D. Gourdon, A.J. Kulik, H.M. Pollock, and G.A.D. Briggs: "How Does a Tip Tap?" *Nanotechnology,* 1997, *8,* pp. 67-75.
56. B.Y. Du, M.R. VanLandingham, Q.L. Zhang, and T.B. He: "Direct Measurement of Plowing Friction and Wear of a Polymer Thin Film Using the Atomic Force Microscope," *J. Mater. Res.,* 2001, *16,* pp. 1487-92.
57. B. Skarman, L.R. Wallenberg, S.N. Jacobsen, U. Helmersson, and C. Thelander: "Evaluation of Intermittent Contact Mode AFM Probes by HREM and Using Atomically Sharp CeO2 Ridges as Tip Characterizer," *Langmuir,* 2000, *16,* pp. 6267-77.
58. H.-Y. Nie, M.J. Walzak, and N.S. McIntyre: "Bilayer and Odd-Numbered Multilayers of Octadecylphosphonic Acid Formed on Si Substrate Studied by Atomic Force Microscopy," *Langmuir,* 2002, *18,* pp. 2955-58.